Journal of Archaeological Science 40 (2013) 4785–4792

Contents lists available at ScienceDirect

Journal of Archaeological Science

journal homepage: http://www.elsevier.com/locate/jas

5,000 years old Egyptian iron beads made from hammered meteoritic iron

Thilo Rehren [a,*], Tamás Belgya [b], Albert Jambon [c], György Káli [d], Zsolt Kasztovszky [b], Zoltán Kis [b], Imre Kovács [e], Boglárka Maróti [b], Marcos Martinón-Torres [f], Gianluca Miniaci [f,g], Vincent C. Pigott [a], Miljana Radivojević [f], László Rosta [d], László Szentmiklósi [b], Zoltán Szőkefalvi-Nagy [e]

[a] UCL Qatar, a UCL Department at Hamad bin Khalifa University, Georgetown Building, PO Box 25256, Doha, Qatar
[b] Centre for Energy Research, Hungarian Academy of Sciences, Budapest, Hungary
[c] Université Pierre et Marie Curie, Paris, France
[d] Institute for Solid State Physics and Optics, Wigner Research Centre for Physics, Hungarian Academy of Sciences, Budapest, Hungary
[e] Institute for Particle and Nuclear Physics, Wigner Research Centre for Physics, Hungarian Academy of Sciences, Budapest, Hungary
[f] UCL Institute of Archaeology, London, UK
[g] UCL Petrie Museum of Egyptian Archaeology, London, UK

ARTICLE INFO

Article history:
Received 14 April 2013
Received in revised form
1 June 2013
Accepted 3 June 2013

Keywords:
Meteoritic iron
Egypt
Beads
Neutron methods
X-ray methods

ABSTRACT

The earliest known iron artefacts are nine small beads securely dated to circa 3200 BC, from two burials in Gerzeh, northern Egypt. We show that these beads were made from meteoritic iron, and shaped by careful hammering the metal into thin sheets before rolling them into tubes. The study demonstrates the ability of neutron and X-ray methods to determine the nature of the material even after complete corrosion of the iron metal. The iron beads were strung into a necklace together with other exotic minerals such as lapis lazuli, gold and carnelian, revealing the status of meteoritic iron as a special material on a par with precious metal and gem stones. The results confirm that already in the fourth millennium BC metalworkers had mastered the smithing of meteoritic iron, an iron–nickel alloy much harder and more brittle than the more commonly worked copper. This is of wider significance as it demonstrates that metalworkers had already nearly two millennia of experience to hot-work meteoritic iron when iron smelting was introduced. This knowledge was essential for the development of iron smelting, which produced metal in a solid state process and hence depended on this ability in order to replace copper and bronze as the main utilitarian metals.

1. Introduction and archaeological background

The production of iron metal from ore only started in the mid-second millennium BC, but a number of earlier iron artefacts are known to exist (Waldbaum, 1999, and literature therein), or at least have been claimed at various stages to be early iron artefacts. These could either be made from accidental by-products of copper smelting, or represent meteoritic iron, or be younger iron intruded into older archaeological contexts, such as the alleged 6th millennium iron object from Samarra (Herzfeld, 1930), later dismissed by the excavator as an Islamic intrusion (Herzfeld, 1932). Confusion also exists over objects made from minerals such as magnetite, which can be mistaken to be corroded iron and even exhibit exsolution lamellae which appear in the microscope similar to the famous Widmannstaetten texture of meteoritic iron; this seems to be the case for instance with the nodules reported by Ghirshman (1939: 206) from Tepe Sialk II, identified as magnetite ore by Pigott (1984). Microchemical and metallographic criteria clearly distinguish these different materials (Buchwald, 1975, 1977, 2005), but their investigation requires invasive sampling, which is not acceptable for archaeological finds of such importance and rarity. The nature and origin of mankind's earliest iron artefacts have therefore remained a matter of uncertainty and dispute. The same is true for the set of iron beads reported here ever since their excavation in 1911, in a predynastic cemetery near the village of el-Gerzeh in Lower Egypt (Fig. 1), believed to be the earliest known extant iron artefacts.

* Corresponding author. Tel.: +974 77770275.
E-mail address: th.rehren@ucl.ac.uk (Th. Rehren).

0305-4403
http://dx.doi.org/10.1016/j.jas.2013.06.002

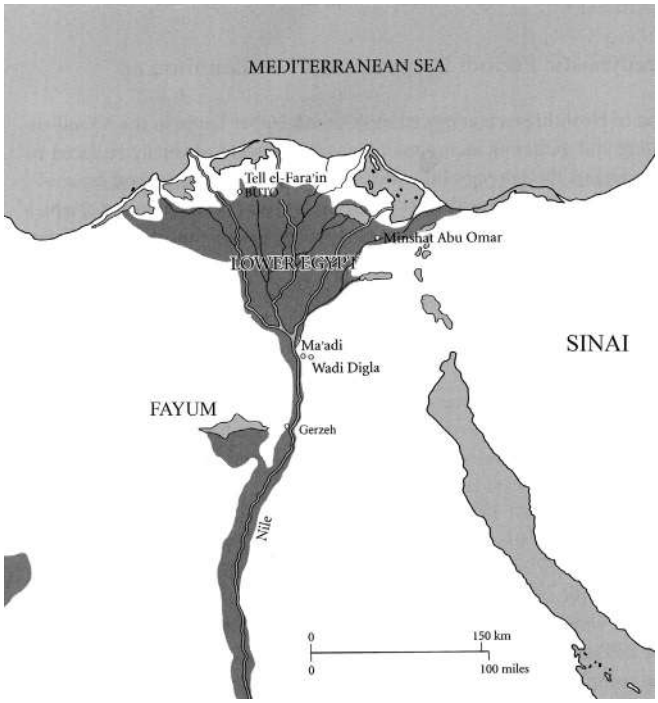

Fig. 1. Map of lower Egypt in the 4th millennium BC, with key predynastic sites marked. Gerzeh is near the entrance to the Fayum. Shaded area indicates cultivated land. Map by Gianluca Miniaci, adapted from Bard (2007).

Fig. 2. Collection of stone and faience beads from Tomb 67. UC10741, modern re-stringing, without the iron beads.

The excavation of these beads was supervised by G.A. Wainwright and J.P. Bushe-Fox as part of investigations in the district of Riqqeh for the Flinders Petrie British School of Archaeology in Egypt (Petrie et al., 1912). Wainwright recorded about 277 burials, securely dated by ceramic and other finds to Naqada Period phases IIC to IIIA, or in terms of absolute chronology about 3400–3100 BC (Stevenson, 2009: 11–31,10: 25).

A total of nine tubular iron beads were retrieved from the cemetery, all from two closed archaeological contexts, and so of secure date. Seven were recorded in tomb 67: three from the waist of the deceased, and four as part of a necklace placed round his neck (Petrie et al., 1912: 15–16). The necklace beads were found in their original order as strung with tubular lapis lazuli, carnelian, agate, and gold beads. Petrie et al. (1912: pl. IV.2) present the necklace beads in order as found; UC10742 is the modern restringing in a different order and excluding the iron beads (Fig. 2). In addition to the beads, tomb 67 contained also a limestone mace-head, a copper harpoon, and a small ivory vessel, a mudstone fish-shaped palette, an ivory spoon, a flint bladelet, two stone vessels, and twelve ceramic vessels (Petrie et al., 1912; Gerzeh tomb card no. 67 in Petrie Museum archive PMA WFP1/103/1/1; Stevenson, 2009: 198, Appendix E under ms 67).

One of the beads had been analysed in the 1920s and found to contain about 7.5 wt% nickel (Desch, 1929; Wainwright, 1932); another analysed later did not yield any nickel (Gowland and Bannister, 1927). More recent analyses of surface samples of three beads by electron microprobe revealed a fully oxidised structure incorporating sand grains (i.e. analysing most likely a secondary corrosion crust rather than the original metal body), with a nickel content below 0.2 wt% (El Gayar, 1995).

The other two iron beads come from grave 133, and according to the report they were placed at the hands of the deceased, but not such that the original order could be determined (Petrie et al., 1912: 16). This tomb contained the largest number of beads and of the most diverse materials in the entire cemetery: lapis lazuli, obsidian, gold, carnelian, calcite, chalcedony, steatite, faience, garnet, and serpentine. In addition the burial equipment included an extraordinary heterogeneous assemblage of artefacts and unworked materials: a porphyry bowl, a miniature pink limestone jar, a bird scutiform-shaped palette, an ivory spoon, a flint flake, an ivory comb (?), shells, a jackal canine tooth, 16 stones of carnelian, green jasper, and quartz, a lump of red resin, and nine pottery vessels (Petrie et al., 1912: 16; Stevenson, 2009: 195–196, Appendix E under ms 133).

The report places particular emphasis on the absence of any signs of plundering or later intrusion in both tombs (Petrie et al., 1912: 16–17): criteria for both tombs include the presence of valuable and unbroken objects; for tomb 67, there is also the preservation of the body in original position, and for tomb 133, where the bones were not well preserved, there was an intact mud coating, two inches thick, over the burial equipment and the body.

The gender of the deceased is not documented: the individual buried in grave 67 is said to belong to a "fair-sized boy" (Petrie et al., 1912: 5) with "a small body" (tomb card) but no more detail can be obtained either from the published report or from the tomb cards. However, both tombs present the widest range of object types in the cemetery, with unusually rich burial equipment and including a number of exotic materials, notably the iron beads. Both the material diversity and the wealth indicate marked social and economic distinction (status and wealth), and perhaps also a specific link to some particular role in specialised networks of exchange relations (Stevenson, 2009: 192–199). As such, the el-Gerzeh beads support the idea that the initial use of a metal, (e.g., iron, copper, gold), is less about exploiting characteristic material properties for functional uses, and more impelled by "the desire for new materials to serve as aesthetic visual displays of identity, whether of a social, cultural or ideological nature" (Roberts et al., 2009: 1019).

Since both tombs are securely dated to Naqada IIC–IIIA, c 3400–3100 BC (Adams, 1990: 25; Stevenson, 2009: 11–31), the beads predate the emergence of iron smelting by nearly 2000 years, and other known meteoritic iron artefacts by 500 years or more (Yalçın 1999), giving them an exceptional position in the history of metal use. Their early date makes it reasonable to assume that they were made from meteoritic iron; however, while the tombs were undisturbed, the intrusion into the tomb of man-made iron through taphonomic processes or contamination during excavation cannot be a priori entirely excluded. Here we present positive proof

of a meteoritic origin of these beads, strengthening the argument that these are indeed the earliest known examples of worked iron metal, and revealing unparalleled information about their manufacturing technology.

2. Materials and methods

We analysed the three beads currently held at the UCL Petrie Museum of Egyptology in London, UK for their chemical composition and metallurgical structure using non-invasive methods (Fig. 3). Bead UC10738 has a maximum length of 1.5 cm and a maximum diameter of 1.3 cm, bead UC10739 is 1.7 cm by 0.7 cm, and bead UC10740 is 1.7 cm by 0.3 cm. All three beads are of rust-brown colour with a rough surface, indicative of heavy iron corrosion. Initial analysis by pXRF indicated an elevated nickel content of the surface of the beads, in the order of a few per cent, and their magnetic property suggested that iron metal may be present in their body (Jambon, 2010).

Meteoritic iron has several characteristics that distinguish it from smelted iron (Buchwald, 1977, 2005; Knox, 1987). Most prominent are the large crystal grain size reaching meter-scale (Buchwald, 1975; cited after Vander Voort, 1992) and Widmannstaetten texture, elevated bulk concentrations of nickel (typically 5 to 10 wt%, but reaching 30 wt% Ni and more, Vander Voort, 1992), cobalt (0.4–1 wt %), phosphorus (0.1–1 wt%), and germanium (mostly 200–400 μg/g), and the presence of mineral phases such as schreibersite and rhabdite ($[Fe,Ni]_3P$), cohenite ($[Fe,Ni]_3C$), troilite (FeS) and sphalerite (ZnS). Some of these characteristics, however, are not diagnostic. While germanium has not been found in smelted iron above c 10 μg/g, nickel and cobalt are common alloying elements in modern steel, and have been found in similar concentrations in some ancient smelted iron (Photos, 1989). Similarly elevated phosphorus concentrations are also found in some smelted iron. Curatorial considerations prevented us from attempting invasive analysis, traditionally necessary to obtain microstructural information or bulk compositional data. Pure surface analyses, such as by XRF analysis of the corrosion-covered surface, was unlikely to provide conclusive evidence about the bulk composition though, requiring the use of non-invasive methods instead that would still provide information about the entirety of the beads, and not just their near-surface area.

Using an access agreement for cultural heritage material under the EU-funded CHARISMA programme, we obtained permission from the Petrie Museum and the UK authorities to take the beads to Budapest, Hungary, for a series of measurements. Neutron-based and X-ray based analytical methods such as prompt-gamma activation analysis (PGAA), particle-induced X-ray emission (PIXE), neutron radiography (NR), and time-of-flight neutron diffraction (ToF-ND) were used to characterise surface and body of the beads, at the laboratories of the Centre for Energy Research and Wigner Research Centre for Physics, Hungarian Academy of Sciences.

Fig. 3. Photographs of three of the originally nine iron beads from Gerzeh, Lower Egypt. From left UC10738, UC10739 and UC10740. © Petrie Museum of Egyptian Archaeology. Photo by Gianluca Miniaci.

2.1. PGAA

Prompt gamma activation analysis (PGAA or PGNAA, Révay and Belgya, 2004) is a nuclear analytical technique for non-destructive quantitative determination of elemental compositions, and has been successfully applied to characterise archaeological objects made of various rocks (Kasztovszky et al., 2008), glass (Kasztovszky and Kunicki-Goldfinger, 2011), as well as metals (Rogante et al., 2010). In this study, it was used to determine the bulk composition of the entire beads rather than just the surface composition. For analysis, the sample is irradiated in a beam of slow (i.e. low energy) neutrons and the gamma-rays from the radiative capture are detected. Since neutrons can go as deep as a few centimeters underneath the surface, PGAA of sufficiently small objects provides bulk composition characteristic for the entire volume. Contrary to the conventional neutron activation analysis (NAA), the irradiation and the detection occur simultaneously. The energies and intensities of the peaks in the gamma spectra are independent of the chemical state of the material; hence the analytical result is free of matrix effects. In most cases, major components and a few significant trace elements can be quantified from one spectrum; unfortunately, the expected diagnostic levels of platinum group elements in meteoritic iron are too low for detection by PGAA.

The present measurements were carried out at the PGAA experimental station of the Budapest Neutron Centre (Szentmiklósi et al., 2010). The intensity of the neutron beam, characterised by the thermal equivalent flux, was about 8×10^7 cm^{-2} s^{-1}. The Compton-suppressed HPGe detector has been precisely calibrated (Belgya and Révay, 2004; Fazekas et al., 1999; Molnar et al., 2002). The gamma-ray spectra were evaluated using the Hypermet-PC program (Révay et al., 2005). The spectroscopic data library used in the analysis was established earlier at the Centre for Energy Research (Révay and Molnár, 2003; Révay et al., 2004). The composition of the analysed samples was determined using the methods described in Révay (2009), while the uncertainties of the concentrations were calculated according to ISO GUM (1995) and Révay (2006).

Due to the elevated germanium background (about 1000 μg/g) caused by the detector crystal itself, this PGAA setup has an unusually high detection limit for germanium; accordingly, our test analyses did not show a significantly higher response for this element for a small piece of known meteoritic iron than for fully corroded smelted iron.

2.2. Neutron radiography

Neutron radiography is based on the attenuation of a neutron beam. Radiography is a direct imaging technique, where the visual representation of an object is obtained non-destructively by detecting the modification of an incident beam as it passes through the matter (Banhart, 2008; Anderson et al., 2009). The interactions between the radiation and the object determine the contrast, revealing the internal structure of the sample.

A setup called NORMA was recently installed at the Budapest Neutron Centre as a part of the NIPS experimental station (Szentmiklósi et al., 2013), where the thermal equivalent flux of the guided cold neutron beam is about 2×10^7 cm^{-2} s^{-1} and the cross-sectional area of the neutron beam is 40×40 mm^2.

The sample was positioned on an xyz sample stage downstream of the neutron collimators, and the transmitted neutrons created

signals in a two-dimensional position sensitive detector (a ^{6}Li-doped ZnS scintillator coupled to a Peltier-cooled Andor CCD camera) located behind the sample. The spatial resolution (about 330 μm) of the imaging system was limited by the divergence of the neutron beam (L/D = 233). The raw two-dimensional digital image was corrected with the open beam profile recorded in the absence of the sample (to compensate for the spatial inhomogeneity of the beam) and also with the dark image recorded with closed neutron beam.

2.3. ToF-ND

The ToF-ND at the Budapest Neutron Centre is a high-resolution time-of-flight powder diffractometer. The fast double choppers can produce as short as 10 μs neutron pulses; the total flight path of neutrons to the detectors is 25 m. In the highest resolution mode and back scattering geometry diffraction spectra with peak widths of 1.5×10^{-3}Å can be collected. The data acquisition is solved by an event recorder: all the event (neutron capture, chopper signs and any external signal) is registered together with a time stamp to a file. In the present experiment the beads were individually placed in cylindrical capsules made of thin Teflon foil and rotated continuously around their longitudinal axis (due to curatorial concerns three-dimensional rotation was avoided); signals of the incremental rotary encoder were registered as well. This method would have allowed to record Bragg-diffraction peaks, i.e. the angular distributions of grains' orientations, thus separating larger crystallites from powder-like phases. However, no such crystal grains could be observed. The instrument is generally used to investigate much larger samples; to increase sensitivity in this case we applied very long measuring times, so that the detectable absolute mass of iron in its metallic form was as low as about 10 mg, i.e. less than 0.1% of the measured sample mass.

2.4. PIXE

External milli-beam particle induced X-ray emission spectroscopy (PIXE) is one of the most powerful and popular methods for non-destructive elemental analysis of precious art and archaeological objects (Gyódi et al., 1999). In this technique selected spots on an object of practically any size and shape are bombarded by energetic protons, and the characteristic X-rays produced are used for quantitative analysis of the irradiated volume. Taking into account both the slowing down of the bombarding protons in the sample and the attenuation of the out-coming X-rays the method is inherently sensitive only for the surface region of depths up to some tens of micrometres, depending on the composition of the sample, the proton energy and the energy of the characteristic X-rays. In standard detection arrangement elements from Al to U can be detected simultaneously, in favourable conditions down to μg/g sensitivities (Johansson et al., 1995). Our PIXE measurements were performed at the 5 MV Van de Graaff accelerator of the Wigner Research Centre of the Hungarian Academy of Sciences, Institute of Particle and Nuclear Physics. The properly collimated proton beam of 2.5 MeV energy was extracted from the evacuated beam pipe to air through a 7.5 μm thick Kapton foil. Target-window distance of 10 mm was chosen for the measurements at which point the beam diameter was found to be about 1.5 mm. The objects to be analysed were fixed to a micro-manipulator to facilitate accurate three-dimensional positioning. External beam currents in the range of 1–10 nA were generally used. The characteristic X-ray spectra were recorded by a computer controlled Amptek X-123 spectrometer with an SDD type detector of 25 mm^2 × 500 μm active volume positioned at 135° with respect to the beam direction. The energy resolution was 130 eV for the Mn Kα line. The net X-ray peak intensities and the concentration calculations were made by the off-line GUPIX program package (Campbell et al., 2000).

3. Results

The ToF-ND testing for grain size and crystal lattice structure of any metallic phases present in the beads found no metallic form of iron in any of the three beads. No definite Bragg peaks were observed, consequently they should consist of a larger number of low symmetry crystalline phases (probably with non-uniform chemical compositions), imperfectly crystallised or amorphous compounds (such as iron hydroxides) and/or hydrogen in any other form. This is considered typical for the corrosion products of iron, and the absence of metallic iron above the detectable minimum mass of about 10 mg indicates that the samples are to more than 99.9% corroded, with virtually no metallic form of iron remaining. The noticeable magnetism of the beads is probably due to the presence of magnetite (Fe_3O_4), a common corrosion product of metallic iron.

Neutron radiography revealed the original shapes and bulk morphology of the artefacts and details of their manufacture. All three artefacts are tubular beads with a central hole along their long axis to facilitate stringing. These holes were not visible during visual inspection due to the corrosion of the beads filling the holes with corrosion products. The NR images demonstrate that the beads were made from rolled-up iron sheet, with areas of overlapping metal visible at the centre of the seam and V-shaped tapering at one end of bead UC10740 (Fig. 4, top). The irregular cross section of the central holes, with several kinks visible also in the inner circumference of UC10738 (Fig. 4, bottom), rule out that the perforation was made by drilling.

PGAA showed that the beads consist predominantly of iron and oxygen in broadly similar amounts, which is consistent with their fully corroded state as indicated by visual inspection and Neutron Diffraction. Of more interest, the beads contain between 2.8 and 4.1 wt% nickel in the corroded material. We assume that about 45% by weight of the current material is hydrogen, oxygen and other light elements such as silicon and calcium that were incorporated during the corrosion process. If we re-calculate the pure transition metal content back to 100%, then these values are equivalent to about 6–9 wt% Ni in solid metal. This assumes that the corrosion

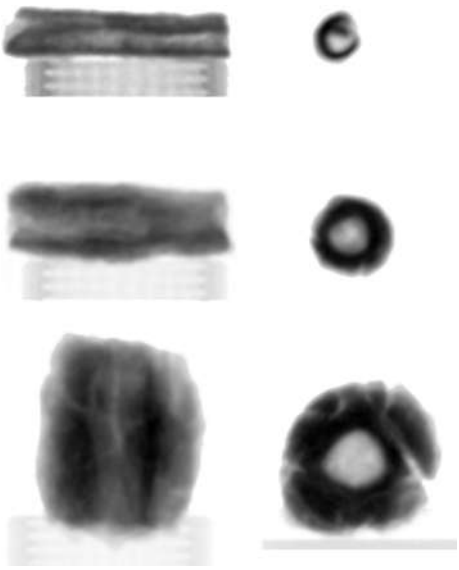

Fig. 4. Neutron images of the three iron beads, in side view (left) and perpendicular (right). UC10740, UC10739 and UC10738 (from top).

does not selectively enrich or deplete one metal over the others, which is a crude assumption; thus, the calculated original concentrations can only be seen as best estimates. In addition, the beads contain 0.6–1.0 wt% phosphorus and 1700–2400 μg/g cobalt, equivalent to c 3600–5100 μg/g Co in the un-corroded metal. Small amounts of light elements (hydrogen to manganese) are thought to represent corrosion and soil particles incorporated from the burial environment (Table 1). We could not determine bulk germanium levels by PGAA due to the germanium content of the detector, resulting in a detection limit as high as 1000 μg/g.

PIXE analysis of the beads' surfaces confirmed the presence of iron as the main element, followed by nickel at an estimated 5 wt%, and the light elements from the soil. Individual spots have different concentrations of copper, lead, arsenic, zinc and manganese, reaching several hundreds of μg/g. Two of the three beads showed spots with germanium above the detection limit (Fig. 5), estimated to be at c 30 μg/g, and reaching up to c 100 μg/g in individual spots.

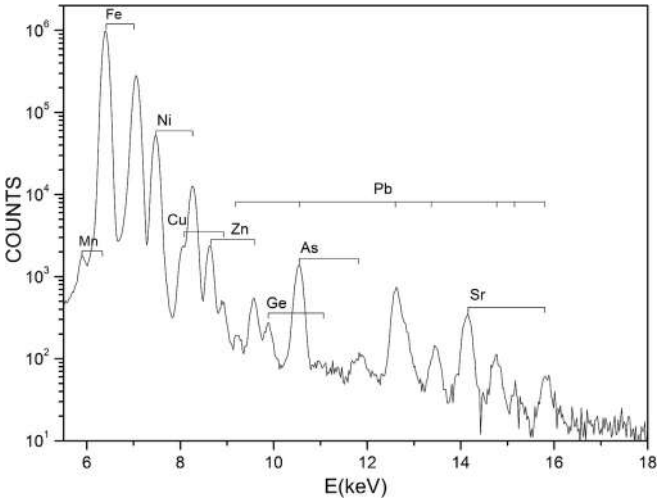

Fig. 5. PIXE spectrum of bead UC10740, showing Kα and Kβ lines for main elements, including iron (Fe), nickel (Ni), and germanium (Ge).

4. Discussion

The bulk contents of the beads in iron, nickel and cobalt are consistent with the assumption that the beads were made from meteoritic iron (Rehren et al., 2012), even though the possible shift in nickel/iron and cobalt/iron ratios during corrosion makes it impossible to determine the original nickel and cobalt content of the metal. The recalculated values for the un-corroded iron beads, given above as 6 to 9 wt% Ni and 0.4 to 0.5 wt% Co, match the typical values of hexahedrite (5–6 wt% Ni) and octahedrite (5–10 wt% Ni) meteorites, the two most common types of iron meteorites.

The most surprising findings of our study are the neutron radiography images showing the delicate rolled sheet-like internal structure of the beads, which was preserved in spite of their complete corrosion (see Fig. 2). Beads UC10739 and UC10740 were made from sheets of approximately 1.7 cm by 2.2 cm and 1.7 cm by 1 cm respectively, with an estimated thickness of probably less than 2 and 1 mm, respectively. The occurrence of these beads as part of a stringed necklace of various materials had quite sensibly been always taken as evidence for their tubular nature, but the complete corrosion state had made it impossible to demonstrate whether they were made by drilling, as with the accompanying stone beads, or from sheet metal, as with the gold beads. Rolling thin metal sheet into tubular beads, including intermittent annealing, is a well-established practice for the early prehistoric production of native metal beads, going back to the ninth millennium BC in Neolithic Anatolia (Maddin et al., 1999; Yalçın and Pernicka, 1999; Birch et al., 2013). However, forming such rolled sheet beads out of coarse-grained and rather hard and brittle meteoritic iron would have required very careful hammering of the metal, most likely with intermittent annealing to first create and then roll the sheet without cracking it. The successful prehistoric use of this manufacturing method for meteoritic iron has recently been documented and experimentally re-created for pre-Columbian Hopewellian beads (McCoy et al., 2008), using machined meteoritic iron sheet that was then reduced by hammering from 5 mm to 4 mm thickness (McCoy pers. comm. 2012). In the Gerzeh samples, this hammering and rolling of iron was done at a much finer scale producing iron sheet as thin as one millimetre or less for bead UC10740, producing long thin tubes with the metal sheet overlapping at the seams. This not only demonstrates a very high level of skill of the pre-dynastic smiths creating these beads, but also suggests that repeated cycles of annealing and hammering were necessary to achieve such thin metal sheet.

Table 1
Composition of three iron beads from Gerzeh (UC10738-40), one partly corroded piece of meteoritic iron from Argentina (CdC3C), and two completely corroded medieval non-meteoritic iron samples (28848/12 and/1) for comparison. All data in weight percent, determined by PGAA. D.L. stands for detection limit.

Sample code element	D.L./ wt%	UC10738		UC10739		UC10740		CdC3C		28848/12		28848/1	
		Conc./ wt%	Abs. unc. ±	Conc./ wt%	Abs. unc. ±	Conc./ wt%	Abs. unc. ±	Conc./ wt%	Abs. unc. ±	Conc./ wt%	Abs. unc. ±	Conc./ wt%	Abs. unc. ±
H	0.0006	1.65	0.03	1.58	0.03	2.03	0.03	0.114	0.003	1.16	0.03	1.36	0.03
B	0.00005	0.0473	0.0009	0.0575	0.0010	0.0810	0.0012	<D.L.		0.00172	0.00004	0.00465	0.00010
Na	0.09	0.13	0.01	0.23	0.02	0.20	0.01	<D.L.		0.059	0.004	0.090	0.012
Mg	0.2	0.66	0.09	<D.L.		0.46	0.04	<D.L.		0.37	0.06	0.47	0.06
Al	0.05	0.18	0.07	0.31	0.02	0.10	0.03	<D.L.		0.12	0.02	0.06	0.02
Si	0.1	1.5	0.1	3.0	0.1	1.3	0.05	<D.L.		0.6	0.04	0.2	0.06
P	0.2	0.8	0.2	0.6	0.1	1.0	0.1	0.24	0.05	<D.L.		<D.L.	
S	0.05	0.2	0.02	0.2	0.01	0.2	0.01	0.11	0.01	0.063	0.007	<D.L.	
Cl	0.005	0.709	0.017	0.625	0.011	0.806	0.015	0.0050	0.0001	0.118	0.003	0.167	0.004
K	0.01	0.028	0.002	0.077	0.003	0.080	0.005	<D.L.		0.023	0.003	0.021	0.004
Ca	0.1	0.48	0.03	0.55	0.02	0.67	0.03	<D.L.		0.80	0.03	0.28	0.02
Ti	0.003	0.016	0.002	0.047	0.002	0.009	0.001	<D.L.		<D.L.		<D.L.	
Mn	0.008	0.023	0.003	0.0160	0.0004	0.050	0.001	<D.L.		0.008	0.0005	0.027	0.0007
Fe	0.2	50.2	0.4	48.7	0.4	48.5	0.3	64.1	0.2	60.2	0.2	60.0	0.2
Co	0.005	0.203	0.006	0.237	0.008	0.170	0.006	0.284	0.010	<D.L.		<D.L.	
Ni	0.2	3.55	0.10	4.10	0.10	2.75	0.06	4.88	0.15	<D.L.		<D.L.	
O (calculated)		39.6	0.1	39.7	0.1	41.6	0.1	30.3	0.1	36.5	0.1	37.3	0.1

The presence of iron phosphide crystals, either as coarse rounded grains of schreibersite or as prismatic rhabdite, is one of the characteristic features of meteoritic iron, resulting from a typical phosphorus content of around 0.3 wt%. We therefore paid particular attention to the possible presence of iron phosphide phases and the total phosphorus content of the beads. First, we studied a small piece of corroded meteoritic iron to gain an impression about the long-term corrosion behaviour of meteoritic iron and to see whether the phosphide crystals can survive corrosion better than the metal matrix. For this, we selected material from the *Campo del Cielo* meteorite field in Argentina that is thought to have fallen about 4000–5000 years ago, i.e. broadly contemporary to the deposition of the iron beads from Gerzeh. Fig. 6 shows that the corrosion penetrates deeply into the metal, with a preferential corrosion of the bulk iron-nickel matrix and at least partial survival of prismatic rhabdite $(Fe,Ni)_3P$ crystals. However, our analyses of the beads from Gerzeh showed no presence of metallic phases above the estimated detection limit of about 10 mg in any of the beads, but bulk phosphorus content several times higher than expected for meteoritic iron. This discrepancy can be explained by the manufacturing method revealed by neutron imaging, and post-depositional processes during corrosion. Repeated heating and hammering of meteoritic iron probably would have destroyed the iron phosphide crystals, partly homogenising the phosphorus content across the worked metal (McCoy et al., 2008); this may well explain why neutron diffraction did not find evidence for the presence of these more corrosion-resistant phases. The higher than expected levels of phosphorus are probably due to the position of the beads in a tomb containing a large amount of decaying organic matter (the grey matter of the brain is particularly rich in phosphorus), and the easy precipitation and enrichment of phosphorus on corroding iron artefacts as iron phosphate.

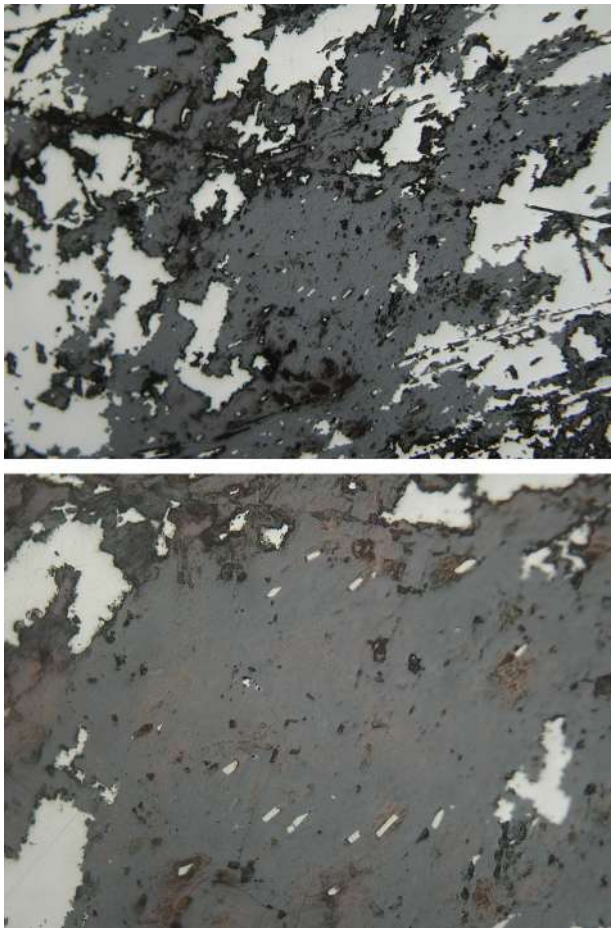

Fig. 6. Micrographs of the corroded meteoritic iron from the Campo del Cielo fall, Argentina. Note the preferential preservation of the prismatic rhabdite crystals (white small angular particles) in the matrix of corroded iron-nickel (grey). Large white areas are un-corroded iron-nickel matrix. Width of image c 1 mm (top) and 0.2 mm (bottom).

So far, the analyses have found no evidence against a possible meteoritic origin of the iron beads from Gerzeh, and good indication for such an origin. Conclusive proof in our view comes from the germanium levels as found by PIXE in selected areas on the surface of two of the three beads. These reach up to c 100 μg/g of corroded material in selected spots on two of the three beads, about half the level common for meteorites and much higher than those detected in smelted iron. We were unable to find literature on the long-term corrosion behaviour of germanium in iron artefacts. However, from theoretical considerations it is very unlikely that germanium would be present in the burial environment in sufficient concentrations to lead to such high levels in the analysed beads. In contrast, we explain the relatively lower level of germanium compared to fresh meteoritic iron with the selective oxidation and subsequent loss of germanium during smithing. It is hoped that experimental work with meteoritic iron and traditional manufacturing methods will in the future produce some information on this issue; until then, we interpret the analysed germanium concentrations as strong proof for a meteoritic origin of the beads, despite the discrepancies in absolute concentrations.

Several other trace elements were detected in the beads, such as copper, zinc, arsenic and lead at levels not present in meteoritic iron similar to those found on the surface of the archaeological beads. PIXE found significant amounts of these elements whereas PGAA did not detect them; this can be due to either the higher detection limits of PGAA for these elements, and/or their presence mostly at the surface. We assume that the presence of copper, arsenic and possibly lead is a consequence of environmental contamination and electrochemical precipitation onto the corroding iron beads, probably from the large copper harpoon found in the same tomb; such precipitation has been shown for early iron objects found in a tomb rich in copper artefacts (Merkel and Barrett, 2000). Alternatively, they could originate from contamination by copper tools used in the manufacture of the beads, as tongs to manipulate the metal during hot hammering or as a temporary core material around which the metal was rolled to shape the tubes. An environmental origin is assumed for boron and chlorine, both common in the saline soils of Egypt's desert into which the tombs were dug. The zinc content is inconclusive; it can either be due to environmental contamination or stem from zinc sulphide inclusions present in the original meteoritic metal.

5. Conclusion

The composition of the beads is consistent with a meteoritic origin of the metal. The germanium content is the strongest indication for this, despite the irregular and relatively low concentrations found. The content in nickel and cobalt, estimated to have been around 6–9 wt% Ni and between 0.4 and 0.5 wt% Co in the original metal, is also strong indication of a meteoritic origin. We explain the presence of elements not consistent with a meteoritic origin, such as copper, arsenic and lead, by environmental contamination, particularly from the corrosion of a large copper artefact near-by. The shape of the beads was obtained by smithing and rolling, most likely involving multiple cycles of hammering and annealing, and not by the traditional stone-working techniques such as carving or drilling used for the other tubular beads from this tomb. Beads UC10739 and UC10740 were made from sheets a few cm square in size with an

estimated thickness of around 1 or 2 mm. No metal structure was identified by the non-invasive methods used, indicating complete corrosion of the beads. It is assumed that re-crystallisation and homogenisation during hammering and annealing of the meteoritic iron into sheet metal would have removed much of the original structure already prior to corrosion. Cycles of hammering and annealing were used previously for producing similar beads during the Neolithic and Early Bronze Age using soft metals such as pure copper and native gold; however, these beads are to our knowledge the earliest smithed iron artefacts known that were made from nickel-rich coarse-grained iron metal, a material much more difficult to work. Composition and manufacturing technique are not compatible with a sub-recent origin of the beads, confirming the archaeological observation by the excavators that they are not later intrusions into the Gerzeh tombs, but indeed humankind's oldest known iron artefacts. Significantly, this is the first multi-analytical study to show that already the earliest known iron artefacts were manufactured with a set of techniques that were to become essential for the processing of bloomery iron, produced in the solid state and hence similar to the meteoritic iron that underpinned the first two millennia of iron metallurgy.

Author contributions

Albert Jambon stimulated the study and performed the initial pXRF analyses on the beads. Thilo Rehren, Marcos Martinón-Torres and Zsolt Kasztovszky designed the study. Thilo Rehren and Zsolt Kasztovszky coordinated and oversaw the individual elements of it. Imre Kovács and Zoltán Szőkefalvi-Nagy performed the PIXE experiments and interpreted the results. György Káli performed the ToF-ND measurements and data evaluation. László Rosta interpreted the results. Zsolt Kasztovszky and Boglárka Maróti performed and evaluated PGAA experiments and interpreted the results. Zoltán Kis, Tamás Belgya and László Szentmiklósi performed and evaluated neutron radiography and interpreted the results. Gianluca Miniaci researched the excavation history and context of the beads. Marcos Martinón-Torres, Vincent Pigott and Miljana Radivojević contributed to the literature research on early iron and overall interpretation of the results. Thilo Rehren wrote the main draft of the manuscript, and all authors contributed to the writing of the text and approved the final manuscript.

Acknowledgements

We acknowledge the CHARISMA project (Grant agreement no.: 228330) for beam time at the BNC in December 2011, and NKTH NAP VENEUS (OMFB-00184/2006), NKTH Gábor Baross grant (REG_KM_09-1-2009-0007) for funding the PGAA and NORMA instruments. The beads used for this study are held at the UCL Petrie Museum of Egyptian Archaeology, which also facilitated and partly funded the transport of the beads for analysis. Comments from three reviewers helped us to improve the manuscript, and are gratefully acknowledged; any remaining errors of fact or interpretation are ours.

Note added in proof stage: We are delighted to see that our results have been corroborated by a more recent study done on another bead from this tomb, currently held at The Manchester Museum (Johnson et al., 2013).

References

Adams, B., 1990. Ancient Nekhen. Garstang in the City of Hierakonpolis (New Malden).
Anderson, I.S., McGreevy, R.L., Bilheux Hassina, Z. (Eds.), 2009. Neutron Imaging and Applications: a Reference for the Imaging Community. Springer.
Banhart, J. (Ed.), 2008. Advanced Tomographic Methods in Materials Research and Engineering. Oxford Univ. Press, Oxford.
Bard, K., 2007. An Introduction to the Archaeology of Ancient Egypt. Wiley-Blackwell, Oxford.
Belgya, T., Révay, Zs., 2004. Gamma-ray spectrometry. In: Molnár, G.L. (Ed.), Handbook of Prompt Gamma Activation Analysis with Neutron Beams. Kluwer, Dordrecht/Boston/New York, pp. 71–111.
Birch, T., Rehren, Th., Pernicka, E., 2013. The metallic finds from Çatalhöyük: a review and preliminary new work. In: Hodder, I. (Ed.), Substantive Technologies at Çatalhöyük. Cotsen Institute of Archaeology Press, pp. 307–316.
Buchwald, V.F., 1975. Handbook of Iron Meteorites. University of California Press, Berkely.
Buchwald, V.F., 1977. The mineralogy of iron meteorites. Philosophical Transactions of the Royal Society of London. A, Mathematical and Physical Sciences 286 (1336), 453–491. Mineralogy: Towards the Twenty-First Century.
Buchwald, V.F., 2005. Iron and Steel in Ancient Times. Det Kongelige Danske Videnskabernes Selskab, Copenhagen.
Campbell, J.L., Hopman, T.L., Maxwell, J.A., Nejedly, Z., 2000. The Guelph PIXE software package III: alternative proton database. Nuclear Instruments and Methods in Physics Research B 170, 193–204.
Desch, C., 1929. Reports on the Metallurgical Examination of Specimens for the Sumerian Committee of the British Association. Reports of the British Association for the Advancements of Science.
El Gayar, E.S., 1995. Pre-dynastic iron beads from Gerzeh, Egypt. iams newsletter 19, 11–12.
Fazekas, B., Révay, Zs., Östör, J., Belgya, T., Molnár, G.L., Simonits, A., 1999. A new method for determination of gamma-ray spectrometer nonlinearity. Nuclear Instruments and Methods in Physics Research A 422, 469–473.
Ghirshman, R., 1939. Fouilles de Sialk, vol. I. Geuthner, Paris.
Gowland, H., Bannister, C., 1939. Ancient Egyptian Metallurgy (London).
Gyódi, I., Demeter, I., Hollós-Nagy, K., Kovács, I., Szőkefalvi-Nagy, Z., 1999. External-beam PIXE analysis of small sculptures. Nuclear Instruments and Methods in Physics Research B 150, 605–610.
Herzfeld, E., 1930. Vorgeschichtliche Töpfereien von Samarra. Reimer, Berlin.
Herzfeld, E., 1932. Steinzeitlicher Hügel bei Persepolis. Iranische Denkmäler 1, 1932.
ISO GUM, 1995. ISO Guide to the Expression of Uncertainty in Measurements, corrected and reprinted edition. International Organization for Standardization, Geneva, Switzerland.
Jambon, A., 2010. Report on Analyses Performed at the Petrie Museum. UCL. Report, filed at the UCL Petrie Museum of Egyptian Archaeology.
Johansson, S.A.E., Campbell, J.L., Malmqvist, K.G., 1995. Particle-induced X-ray Emission Spectrometry (PIXE). Wiley.
Johnson, D., Tyldesley, J., Lowe, T., Withers, Ph., Grady, M., 2013. Analysis of a prehistoric Egyptian iron bead with implications for the use and perception of meteorite iron in ancient Egypt. Meteoritics and Planetary Science 48, 997–1006.
Kasztovszky, Zs., Kunicki-Goldfinger, J., 2011. Applicability of prompt gamma activation analysis to glass archaeometry. In: Turbanti-Memmi, I. (Ed.), Proceedings of the 37th International Symposium on Archaeometry. Springer, Berlin/Heidelberg, pp. 83–90.
Kasztovszky, Zs., Biró, K.T., Markó, A., Dobosi, V., 2008. Cold neutron prompt gamma activation analysis – a non-destructive method for characterisation of high silica content chipped stone tools and raw materials. Archaeometry 50, 12–29.
Knox, R., 1987. On distinguishing meteoritic from man-made nickel-iron in ancient artifacts. MASCA Journal 4, 178–184.
Maddin, R., Muhly, J., Stech, T., 1999. Early metalworking at Çayönü. In: Hauptmann, A., Pernicka, E., Rehren, Th., Yalçın, Ü. (Eds.), The Beginnings of Metallurgy. Deutsches Bergbau-Museum, Bochum, pp. 37–44.
McCoy, T.J., Marquardt, A.E., Vicenzi, E.P., Ash, R.D., Wasson, J.T., 2008. Meteoritic metal beads from the Havana, Illinois, Hopewell Mounds: a source in Minnesota and implications for trade and manufacture. Lunar and Planetary Science 39.
Merkel, J., Barrett, K., 2000. 'The adventitious production of iron in the smelting of copper' revisited: metallographic evidence against a tempting model. Historical Metallurgy 34, 59–66.
Molnar, G.L., Révay, Zs., Belgya, T., 2002. Wide energy range efficiency calibration method for Ge detectors. Nuclear Instruments and Methods in Physics Research A 489, 140–159.
Petrie, W.M.F., Wainwright, G.A., Mackay, E., 1912. The Labyrinth, Gerzeh and Mazghuneh, vol. XXI. British School of Archaeology in Egypt, London.
Photos, E., 1989. The question of meteoritic versus smelted nickel-rich iron: archaeological evidence and experimental results. World Archaeology 20, 403–421.
Pigott, V.C., 1984. Āhan "iron" from prehistory to the ethnographic present. Encyclopaedia Iranica. http://www.iranicaonline.org/articles/ahan-iron.
Rehren, Th., Jambon, A., Káli, Gy., Kasztovszky, Zs., Kis, Z., Kovács, I., Maróti, B., Martinón-Torres, M., Pigott, V.C., Quirke, S., Szentmiklósi, L., Szőkefalvi-Nagy, Z., 2012. Mankinds' earliest iron – really meteoritic? In: Braekmans, D., Honings, J., Degryse, P. (Eds.), Book of Abstracts of ISA 2012, the 39th International Symposium on Archaeometry, 28 May – 1 June 2012. Leuven, Belgium, p. 248.
Révay, Zs., Belgya, T., 2004. Principles of PGAA method. In: Molnár, G.L. (Ed.), Handbook of Prompt Gamma Activation Analysis with Neutron Beams. Kluwer, Dordrecht/Boston/New York, pp. 1–30.
Révay, Zs., Molnár, G.L., 2003. Standardisation of the prompt gamma activation analysis method. Radiochimica Acta 91, 361–369.

Révay, Zs., 2006. Calculation of uncertainties in prompt gamma activation analysis. Nuclear Instruments and Methods in Physics Research A 564, 688–697.
Révay, Zs., 2009. Determining elemental composition using prompt gamma activation analysis. Analytical Chemistry 81, 6851–6859.
Révay, Zs., Belgya, T., Molnár, G.L., 2005. Application of Hypermet-PC in PGAA. Journal of Radioanalytical and Nuclear Chemistry 265, 261–265.
Révay, Zs., Firestone, R.B., Belgya, T., Molnár, G.L., 2004. Catalog and Atlas of prompt gamma rays. In: Molnár, G.L. (Ed.), Handbook of Prompt Gamma Activation Analysis with Neutron Beams. Kluwer, Dordrecht/Boston/New York, pp. 173–364.
Roberts, B.W., Thornton, C.P., Pigott, V.C., 2009. Development of metallurgy in Eurasia. Antiquity 83 (322), 1012–1022.
Rogante, M., Kasztovszky, Zs., Manni, A., 2010. Prompt gamma activation analysis of bronze fragments from archaeological artefacts. Notiziario Neutroni e Luce di Sincrotrone 15, 12–23.
Stevenson, A., 2009. The Predynastic Egyptian Cemetery of el-Gerzeh. Social Identities and Mortuary Practices, vol. 186. Orientalia Lovaniensia Analecta, Leuven, Paris, Walpole.
Szentmiklósi, L., Belgya, T., Révay, Zs., Kis, Z., 2010. Upgrade of the prompt gamma activation analysis and the neutron-induced prompt gamma spectroscopy facilities at the Budapest research reactor. Journal of Radioanalytical and Nuclear Chemistry 286, 501–505.
Szentmiklósi, L., Kis, Z., Belgya, T., Révay, Zs., 2013. Prompt gamma activation imaging at the Budapest research reactor. In: Ridikas, D. (Ed.), Report of the IAEA-F1-TM-40776 Catalogue of Products and Services of Research Reactors: Applications of Neutron Beams 5–7 September 2011. IAEA, Vienna, Austria (in press).
Vander Voort, G.F., 1992. A note on metallographic techniques for iron meteorites. Materials Characterization 29, 223–241.
Wainwright, G.A., 1932. Iron in Egypt. Journal of Egyptian Archaeology 18, 3–15.
Waldbaum, J., 1999. The coming of iron in the Eastern Mediterranean: thirty years of archaeological and technological research. In: Pigott, V.C. (Ed.), The Archaeometallurgy of the Asian Old World, Masca Research Papers in Science and Archaeology, vol. 16. The University Museum, University of Pennsylvania, Philadelphia, pp. 27–57.
Yalçın, Ü., 1999. Early Iron Metallurgy in Anatolia. Anatolian Studies 49, 177–187.
Yalçın, Ü., Pernicka, E., 1999. Frühneolithische Metallbearbeitung am Aşıklı Höyük, Türkei. In: Hauptmann, A., Pernicka, E., Rehren, Th., Yalçın, Ü. (Eds.), The Beginnings of Metallurgy. Deutsches Bergbau-Museum, Bochum, pp. 45–54.